

Bayesian Effect Selection for Additive Quantile Regression with an Analysis to Air Pollution Thresholds

Nadja Klein and Jorge Mateu

Nadja Klein is Assistant Professor of Applied Statistics and Emmy Noether Research Group Leader in Statistics and Data Science at Humboldt-Universität zu Berlin; Jorge Mateu is Professor of Statistics within the Department of Mathematics at Universitat Jaume I. Correspondence should be directed to Prof. Dr. Nadja Klein at Humboldt Universität zu Berlin, Unter den Linden 6, 10099 Berlin. Email: nadja.klein@hu-berlin.de.

Acknowledgments: Nadja Klein gratefully acknowledges support by the German research foundation (DFG) through the Emmy Noether grant KL 3037/1-1. Jorge Mateu is partially supported by grants PID2019-107392RB-I00 from Ministry of Science and Innovation, and by UJI-B2018-04 from Universitat Jaume I.

Bayesian Effect Selection for Additive Quantile Regression with an Analysis to Air Pollution Thresholds

Abstract

Statistical techniques used in air pollution modelling usually lack the possibility to understand which predictors affect air pollution in which functional form; and are not able to regress on exceedances over certain thresholds imposed by authorities directly. The latter naturally induce conditional quantiles and reflect the seriousness of particular events. In the present paper we focus on this important aspect by developing quantile regression models further. We propose a general Bayesian effect selection approach for additive quantile regression within a highly interpretable framework. We place separate normal beta prime spike and slab priors on the scalar importance parameters of effect parts and implement a fast Gibbs sampling scheme. Specifically, it enables to study quantile-specific covariate effects, allows these covariates to be of general functional form using additive predictors, and facilitates the analysts' decision whether an effect should be included linearly, non-linearly or not at all in the quantiles of interest. In a detailed analysis on air pollution data in Madrid (Spain) we find the added value of modelling extreme nitrogen dioxide (NO₂) concentrations and how thresholds are driven differently by several climatological variables and traffic as a spatial proxy. Our results underpin the need of enhanced statistical models to support short-term decisions and enable local authorities to mitigate or even prevent exceedances of NO₂ concentration limits.

Keywords: Air pollution; asymmetric Laplace distribution; distributional regression; effect decomposition; NO₂ and O₃; penalised splines; spike and slab prior

1 Introduction

Air quality is deteriorating globally at an alarming rate due to increasing industrialisation and urbanisation (Ryu et al.; 2019). According to the European Environment Agency (EEA; 2020), air pollution is the single largest environmental health risk in Europe, and in many countries worldwide. An expert committee, being part of the British Committee on the Medical Effects of Air Pollutants, estimated in August 2018 that between 28,000 and 36,000 premature deaths may be linked to air pollution in the UK every year (Airquality-News; 2018). This report complies with the study presented in 2018 by European Environment Agency (EEA; 2018), which states that the estimated impacts on the population in 41 European countries of exposure to nitrogen dioxide (NO₂) and ozone (O₃) concentrations in 2015 were around 79,000 and 17,700 premature deaths per year, respectively.

Many European cities still regularly exceed current EU limits for NO₂ (EEA; 2018). Indeed, the Urban NO₂ Atlas (Urban-NO₂-Atlas; 2019) provides city fact-sheets to help designing effective air quality measures with the aim to reduce NO₂ concentration within European cities. The Atlas identifies the main sources of NO₂ pollution for each city, helping policymakers to design target measures and actions against them.

NO₂ is one of a group of gases called nitrogen oxides (NO_x). While all of these gases are harmful to human health and the environment, NO₂ is of greater concern (Valks et al.; 2011; Achakulwisut et al.; 2019) and is mostly emitted into the air through the burning of fuel. NO₂ generates from emissions from cars, trucks and buses, power plants, and off-road equipment (Perez and Trier; 2001; Lee et al.; 2014; Catalano et al.; 2016) and is a primary pollutant. Indeed, as indicated by the European Environment Agency (EEA; 2018), road transport is the largest contributor to NO₂ pollution in the EU, ahead of the energy, commercial, institutional and household sectors. On the other side, the ozone molecules (O₃) are harmful to air quality outside of the ozone layer. O₃ is a so-called secondary pollutant not emitted directly from a source (like vehicles or power plants). O₃ can be “good” or “bad” for health and the environment depending on where it is found in the atmosphere. Stratospheric ozone is “good” because it protects the living organisms from ultraviolet radiation from the sun. Ground-level ozone is a colorless and highly irritating gas that forms just above the earth’s surface. It is “bad” because it can trigger a variety of human health problems, particularly for children, the elderly, and people of all ages who have lung diseases such as

asthma (Valks et al.; 2011). Breathing air with a high concentration of NO₂ can irritate airways in the human respiratory system and can harm our health as well. As the global population becomes more health conscious, various studies have been conducted to determine the effect of NO₂ concentration on human health. High NO₂ concentrations in urban areas cause bronchial and lung cancer and have severe effects on asthmatic patients (Achakulwisut et al.; 2019).

Social medical costs due to NO₂ pollution are certainly high. To reduce these social costs, many countries regulate NO₂ concentration levels using environmental policies targeting at NO₂ reduction (Valks et al.; 2011; Borge et al.; 2018; Ryu et al.; 2019). For example, the EU has established an integrated environmental policy agreement for the transport, industrial, and energy sectors to improve air pollution at national, regional, and local levels. In addition, since 2013, China has sought to install selective catalytic reduction (SCR) equipment in power plants to establish emissions standards to reduce NO₂ levels through the Air Pollution Prevention and Control Action Plan.

However, to establish effective environmental regulations that reduce the impact of NO₂, accurate information on the nature and the way several sources of air pollution interact with and/or produce NO₂ is by all means needed and essential. Modelling air pollution at both global and local scales enables consistent comparisons of relations between air pollution and health. For example, as NO₂ is highly traffic-related and localised, its local understanding is needed for the assessment of personal outdoor exposure, in particular in areas close to sources of the pollutant such as primary roads.

Statistical models for air pollution analysis are under continuous development. Most of the classical approaches are based on regression techniques through linear-based relations (Meng et al.; 2015; Hatzopoulou et al.; 2017; Antanasijevic et al.; 2018; Lua et al.; 2020). In addition, ensemble tree-based (e.g. random forests) and neural network techniques (Ryu et al.; 2019; Prybutok et al.; 2000) have been considered to investigate if more flexible models can better capture non-linear relationships between predictors and NO₂. Regression-based methods fit one model to the entire range of each predictor, while ensemble tree-based methods build on subsets of data and sub-ranges of predictors. The latter methods are representative for the techniques that are evaluated in the most recent air pollution modelling. However, despite the increased flexibility such models lack the possibility to understand and interpret which predictors affect air pollution and in what functional

form (e.g. linearly or non-linearly). Both approaches in addition come with the drawback of modelling the expected NO2 concentration only rather than allowing to directly regress on exceedances over certain thresholds of the entire NO2 distributions. Such thresholds are imposed by authorities to decide on and classify the seriousness of a particular event. From a statistical point of view, these thresholds induce quantiles, and we focus here on this interesting (while not much treated) aspect by using quantile regression models. However, in addition to thereby allowing the predictor effects to differ for distinct quantiles, we develop quantile regression further and facilitate general function selection and effect decomposition (e.g. into respective linear and non-linear parts) in a highly interpretable model.

To determine the influence of covariates $\mathbf{X} = (X_1, \dots, X_p)^\top$ on quantiles of the distribution of a dependent variable $Y \in \mathcal{Y} \subset \mathbb{R}$ directly, an important contribution amongst other functionals beyond the mean (Kneib; 2013) is quantile regression (Koenker; 2005). One of the main advantages over mean regression (McCullagh and Nelder; 1989; Hastie and Tibshirani; 1990) is that quantile regression permits to supply detailed information about the complete conditional distribution instead of only the mean by considering a dense set of conditional quantiles. In addition, outliers and extreme data are usually less influential in quantile regression due to the inherent robustness of quantiles.

Estimation of the conditional τ th quantile of interest, $\tau \in (0, 1)$ in a basic linear quantile regression (QR) model, as proposed in Koenker and Bassett (1978), is based on solving

$$\min_{\beta \in \mathbb{R}^p} \sum_{i=1}^n \rho_\tau(y_i - \mathbf{x}_i \boldsymbol{\beta}), \quad (1)$$

where $\rho_\tau(u) = u(\tau - \mathbb{1}_{\{u < 0\}})$ for $u \in \mathbb{R}$ is the so-called piecewise linear “check function”. This approach is completely non-parametric as it does not make any specific choice about an error distribution. No closed form solution for the minimisation of the above problem exists, but quantile regression (QR) estimates can be obtained based on linear programming.

To be able to handle non-linear or more general functional relationships between response and covariates on conditional quantiles directly, structured additive quantile (STAQ) regression models have been suggested in the literature (Yue and Rue; 2011; Waldmann et al.; 2013). These build on the general idea of structured additive models for mean regression (STAR; Fahrmeir et al.; 2004; Wood; 2017) which can capture not only linear and non-linear shapes of univariate covariates but also spatial effects, interactions, grouping effects and others. While the aforementioned references to STAQ models rely on Bayesian

principles, alternatives have been developed as well (see e.g. Meinshausen; 2006; Koenker; 2010; Fenske et al.; 2011; Koenker; 2011; Fasiolo et al.; 2020).

However, when it comes to variable or effect selection in such STAQ models, literature, becomes much scarcer. Indeed, variable selection for quantile regression has so far mostly been done in the linear case, see for instance Wu and Liu (2009); Alhamzawi (2015) for a few references within a classical frequentist framework and Alhamzawi and Yu (2012, 2013); Yu et al. (2013) for some Bayesian counterparts.

To fill this gap and motivated by our application to air pollution, it is thus the aim of this paper to develop general Bayesian effect selection for STAQ models thereby significantly enriching existing suggestions for linear quantile regression. To achieve this goal, we employ a normal beta prime spike and slab prior on the scalar importance parameters of predictor effect parts Klein et al. (2021) and implement posterior estimation based on efficient Markov chain Monte Carlo (MCMC) simulations. All steps can be realised by Gibbs updates thus being fast to draw samples from the complex posteriors.

Bayesian variable selection based on spike and slab priors has been popularised by Mitchell and Beauchamp (1988) for linear mean regression and was significantly developed further in several contexts (see, for instance, George and McCulloch; 1997); see also Clyde and George (2004); O’Hara and Sillanpää (2009) for some overviews. We believe our approach makes a necessary contribution and specifically enables for three essential features simultaneously: to (i) study quantile-specific covariate effects, (ii) allow these covariates to be of general functional form (e.g. non-linear) using additive predictors, (iii) decide whether an effect should be included linearly, non-linearly or not at all in the relevant threshold quantiles. In our application the latter will be $\tau \in \{0.6, 0.8, 0.9\}$, see Section 2 for more details.

The rest of the paper is structured as follows. Inspired by our application and analysis with background and data treated in Section 2, we detail our methodological approach to Bayesian effect selection in STAQ models in Section 3. While our method can be applied in a wide range of applications, our empirical results in Section 4 quantify the added-value of modelling extreme NO₂ concentrations, and how thresholds inducing conditional quantiles are able to highlight important modelling differences. These results underpin the need of enhanced statistical models to support short-term decisions and enable local authorities to mitigate or even prevent exceedances of NO₂ concentration limits. The paper ends with some conclusions and a discussion in Section 5.

2 The data and research questions

2.1 Air pollution, NO₂ and O₃. Some motivating basics

Air pollution in urban areas is mainly due to the intense use of motorised transport for travelling, in particular private cars and heavy goods vehicles. This is a priority issue for transportation planners and public authorities, given the harmful effects of pollution to human health and the environment (Bergantino et al.; 2013). Nitrogen dioxide (NO₂) along with nitric oxide (NO) reacts with other chemicals in the air to form both particulate matter and ozone. Both of these are also harmful when inhaled due to effects on the respiratory system. NO₂ and NO interact with water, oxygen and other chemicals in the atmosphere to form acid rain. Acid rain harms sensitive ecosystems such as lakes and forests. Breathing air with a high concentration of NO₂ can irritate airways in the human respiratory system. Such exposures over short periods can aggravate respiratory diseases, particularly asthma, leading to respiratory symptoms (such as coughing, wheezing or difficulty breathing), hospital admissions and visits to emergency rooms. Longer exposures to elevated concentrations of NO₂ may contribute to the development of asthma and potentially increase susceptibility to respiratory infections. People with asthma, as well as children and the elderly, are generally at greater risk for the health effects of NO₂.

Ground-level ozone (O₃) is not emitted directly into the air, but is created by chemical reactions between oxides of nitrogen (NO_x) and volatile organic compounds (VOC). This happens when pollutants emitted by cars, power plants, industrial boilers, refineries, chemical plants, and other sources chemically react in the presence of sunlight. Ozone in the air we breathe can harm our health. People with certain genetic characteristics, and people with reduced intake of certain nutrients, such as vitamins C and E, are at greater risk from ozone exposure. Breathing elevated concentrations of O₃ can trigger a variety of responses, such as chest pain, coughing, throat irritation, and airway inflammation. It also can reduce lung function and harm lung tissue. Ozone can worsen bronchitis, emphysema, and asthma, leading to increased medical care.

One of the main problems caused by air pollution in urban areas is photochemical oxidants. Among these, O₃ and NO₂ are particularly important because they are capable of causing adverse effects on human health (WHO; 2014). The formation of O₃ depends on the intensity of solar radiation, the absolute concentrations of NO_x and VOC, and the ratio of

NO_x (NO and NO₂) to VOC (Valks et al.; 2011). NO is converted to NO₂ via a reaction with O₃, and during daytime hours NO₂ is converted back to NO as a result of photolysis, which leads to the regeneration of O₃. However, this phenomenon is not well understood so far. The concentration of photochemical oxidants can be decreased by controlling their precursors: nitrogen oxides NO_x and VOCs. However, the efficiency of emission control also depends on the relationship between primary and secondary pollutants, as well as ambient meteorological conditions.

Clearly, and owing to the chemical coupling of O₃ and NO_x, the levels of O₃ and NO₂ are inherently linked. Therefore, the response to reduction in the emission of NO_x is remarkably non-linear (Valks et al.; 2011; Borge et al.; 2018; Ryu et al.; 2019) and any resultant reduction in the level of NO₂ is invariably accompanied by an increase in the level of O₃. In addition, changes in the level of O₃ on a global scale lead to an increasing background which influences local O₃ and NO₂ levels and the effectiveness of local emission controls.

It is therefore necessary to obtain a thorough understanding of the cross relationship among O₃, traffic flow and NO₂ under various atmospheric conditions to improve the understanding of the chemical coupling among them. The non-linear mechanisms of the interdependencies between O₃ and NO₂ in combination with other pollutants and atmospheric conditions are still not well understood and need further study. These non-linear effects are in line with thresholds that authorities impose on the records of NO₂; environmental pollution alarms are placed upon three different thresholds, 60% (moderate), 80% (large) and 90% (extreme).

2.2 The data

The Surveillance System of the City of Madrid (Spain) keeps a web portal with open data from many sources and environmental problems (see <https://datos.madrid.es/portal/site/egob>). In particular, this system collects through a number of stations basic information for atmospheric surveillance. We focus here on one weather and one pollution station located in downtown Madrid as they are placed in such a particular place of the city that represents one of the peak locations of air pollution and traffic congestion. We have daily data from 1 January 2016 to 31 December 2019 on the three air pollutants NO₂ (*no2*), O₃ (*o3*) and CO (carbon monoxide, *co*), along with a number of climatological variables. For the latter we have daily average precipitation (*prec*), temperature (*temp*),

average wind speed (*vel*), wind gust speed (*racha*), maximum pressure (*pres_max*), and minimum pressure (*pres_min*). In addition, we have information on traffic flow (*traffic*) averaged per day and per street, together with the maximum and minimum per day from 800 streets surrounding the measuring station. Both traffic and pollution data are available <https://datos.madrid.es/portal/site/egob> provided by the Madrid city council.

As noted before, and due to complex chemical reactions, NO₂ is cross linked with O₃ and other pollutants through non-linear forms in such a way that any increase or reduction in the level of O₃ affects the level of NO₂. In this line, we consider the latter as a response variable in our model to fully address these type of relationships for further control strategies.

Table 1 shows a description and summary statistics of the continuous covariates (before standardisation to $[0, 1]$). The year from 2016–2019 is coded as 0/1 dummy variables with 2016 as a reference category.

Variable	Description	Mean	Std	Min/Max
<i>co</i>	carbon monoxide	0.41	0.25	0.00/2.40
<i>o3</i>	ozone	39.57	20.29	0.00/89.00
<i>prec</i>	precipitation	1.01	3.35	0.00/28.50
<i>temp</i>	average temperature	16.40	7.90	2.10/32.90
<i>vel</i>	average wind speed	1.80	1.00	0.00/6.40
<i>racha</i>	wind gust speed	8.94	3.28	1.90/26.10
<i>pres_max</i>	maximum pressure	943.20	5.58	922.00/967.30
<i>pres_min</i>	minimum pressure	938.75	6.17	915.00/957.40
<i>traffic</i>	average traffic flow	776.22	147.36	249.63/1210.22

Table 1: Description and summary statistics of continuous covariates (before standardisation to $[0, 1]$ in the data set. The average traffic is measured as daily average from approximately 800 segments of traffic flow around the Carmen station. In addition, we have the year from 2016–2019 coded as 0/1 dummy variables with 2016 as a reference category.

Figure 1 depicts some preliminary univariate analyses with *o3* as predictor. In particular, we show histograms of the response *no2* according to the *o3*-quartiles, i.e. where $Q(\tau)$, $\tau \in \{0.25, 0.50, 0.75\}$ is the corresponding quartile of the empirical *o3* distribution in panel (a). We also show normalised quantile residuals from the univariate Gaussian regression model (panel (b)). Then, we finally depict the predicted expectation $\mathbb{E}(no2)$ as well as threshold quantiles $\tau \in \{0.6, 0.8, 0.9\}$ obtained from a linear and non-linear Gaussian model, respectively (panels (c) and (d)). In the same line, Figure 2 shows some initial results when using *traffic* as a predictor in a univariate mean regression model. Looking at these two figures, we note that depending on the predictor values, NO₂ distributions differ (see panels

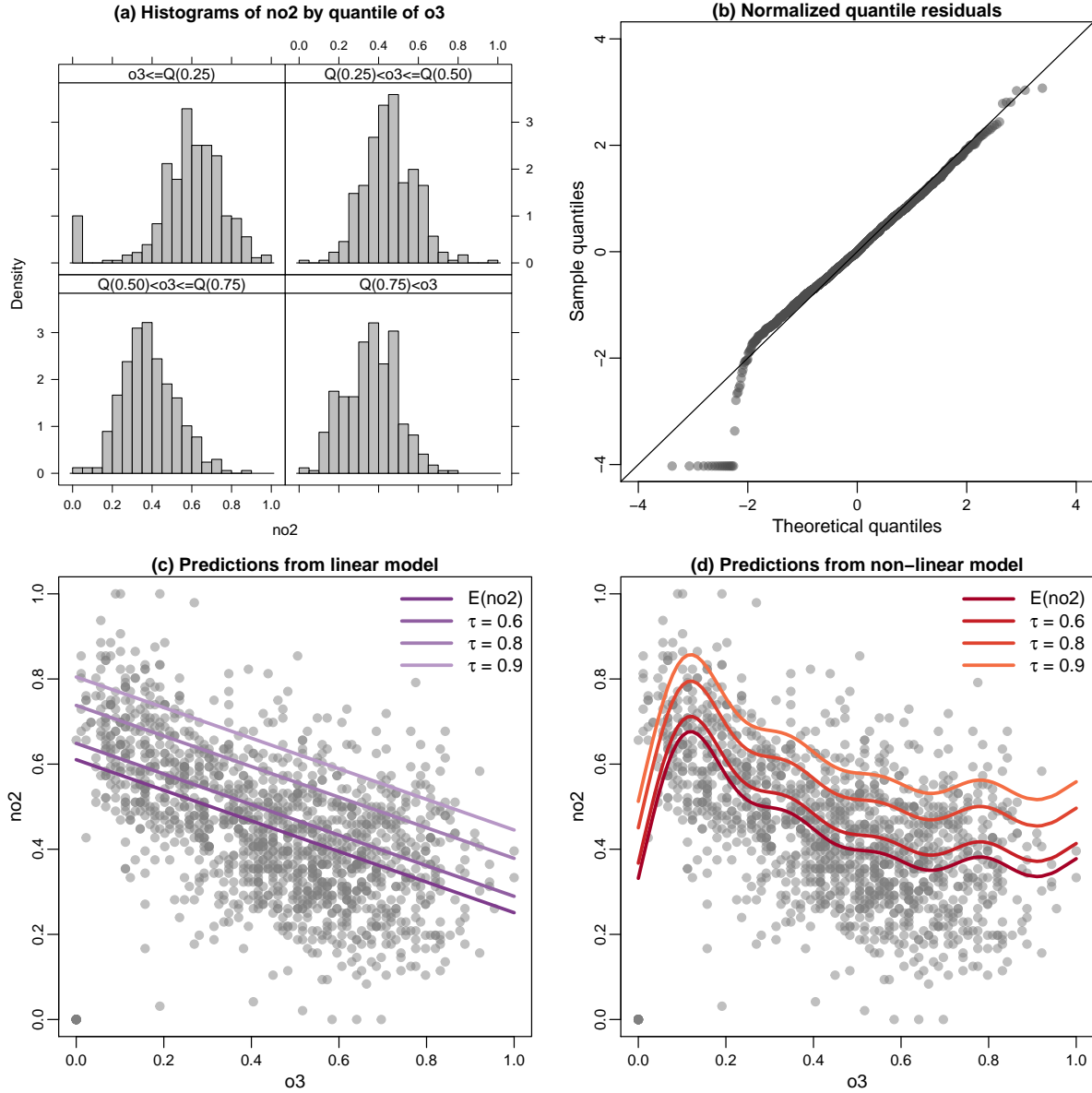


Figure 1: Results from univariate preliminary analyses with o_3 as predictor. Panel (a) shows histograms of the response no_2 according to the o_3 -quartiles, i.e. where $Q(\tau)$, $\tau \in \{0.25, 0.50, 0.75\}$ is the corresponding quartile of the empirical o_3 distribution. Panel (b) shows normalized quantile residuals from the univariate Gaussian regression model. Panels (c) and (d) show the predicted expectation $E(no_2)$ as well as threshold quantiles $\tau \in \{0.6, 0.8, 0.9\}$ obtained from a linear and non-linear Gaussian model, respectively.

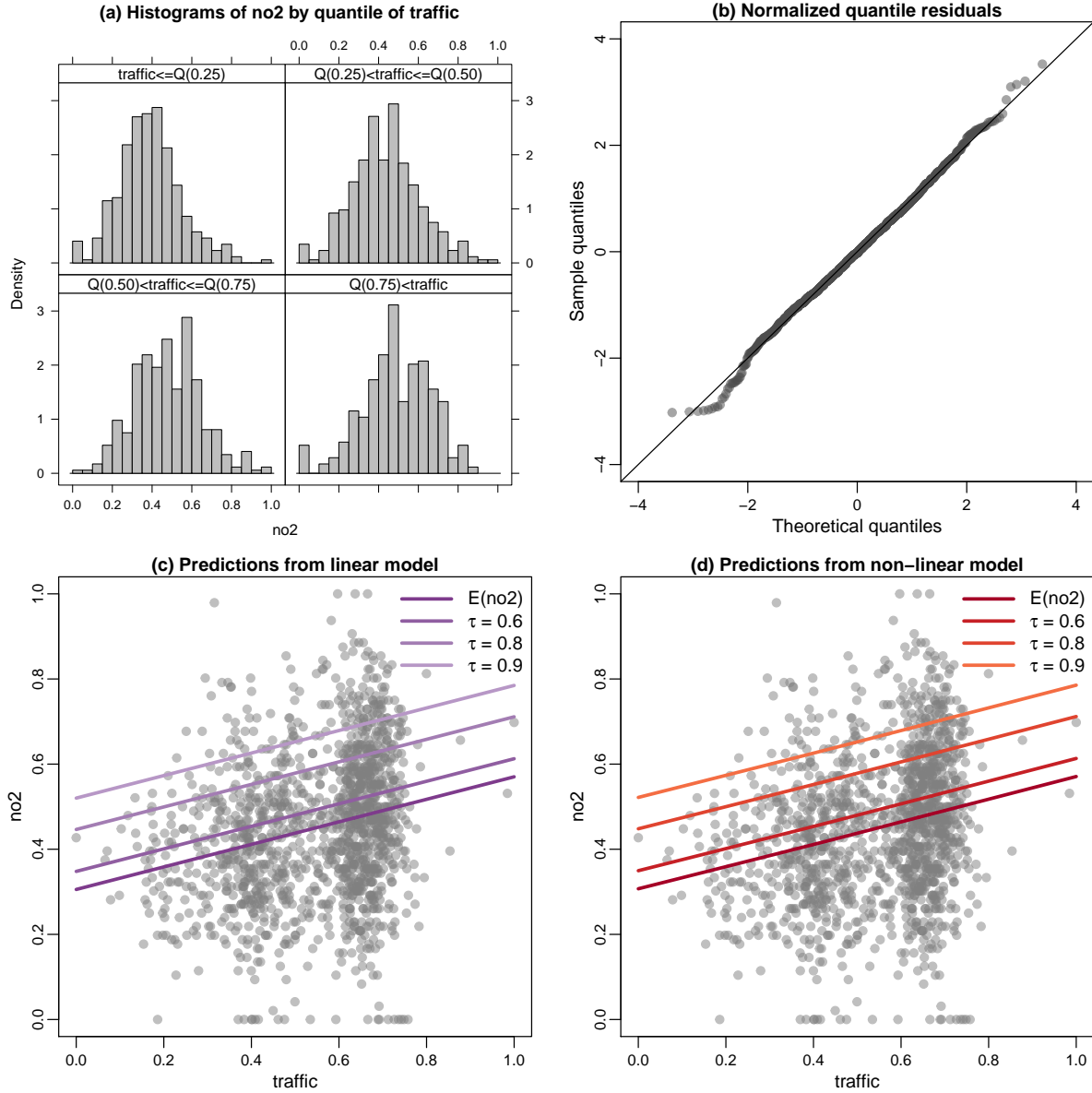


Figure 2: Results from univariate preliminary analyses with *traffic* as predictor. Panel (a) shows histograms of the response *no2* according to the *traffic*-quartiles, i.e. where $Q(\tau)$, $\tau \in \{0.25, 0.50, 0.75\}$ is the corresponding quartile of the empirical *traffic* distribution. Panel (b) shows normalised quantiles residuals from the univariate Gaussian regression model. Panels (c) and (d) show the predicted expectation $E(\text{no2})$ as well as threshold quantiles $\tau \in \{0.6, 0.8, 0.9\}$ obtained from a linear and non-linear Gaussian model, respectively.

(a)), and looking at the tails we note that NO2 distributions are non-Gaussian (see panels (b)). In addition, the quantiles from linear and non-linear regression are parallel, which is not appropriate because conditional on traffic, the variance of NO2 is increasing with increasing traffic. Finally, we observe that the predictor O3 has a clear non-linear effect on NO2, while the one for traffic is rather linear.

3 Bayesian effect selection for additive quantile regression

We first review Bayesian quantile regression using the auxiliary likelihood approach of Yu and Moyeed (2001) with latent Gaussian representation for computational feasibility, before we outline the normal beta prime spike and slab (NBPSS) prior for the quantile-specific regression coefficients. We also study effect decomposition into linear and respective non-linear effect parts as well as a feasible and interpretable way to eliciting hyperparameters of the NBPSS prior.

3.1 Bayesian quantile regression with auxiliary likelihood

Let $(y_i, \boldsymbol{\nu}_i)$, $i = 1, \dots, n$ denote n independent observations on a continuous response variable $Y \in \mathcal{Y} \subset \mathbb{R}$, and $\boldsymbol{\nu}$ the covariate vector comprising different types of covariate information such as discrete and continuous covariates or spatial information, see Section 3.2 for details. We then consider the model formulation

$$y_i = \eta_{i,\tau} + \varepsilon_{i,\tau},$$

where $\eta_{i,\tau}$ is a structured additive predictor (Fahrmeir et al.; 2004) for a specific conditional quantile τ and $\varepsilon_{i,\tau}$ is an appropriate error term. Rather than assuming a zero mean for the errors as in classical mean regression, in quantile regression we assume that the τ th quantile of the error term is zero, i.e., $F_{\varepsilon_{i,\tau}}(0) = \tau$, where $F_{\varepsilon_{i,\tau}}(\cdot)$ denotes the cumulative distribution function of the i th error term. This assumption implies that the predictor $\eta_{i,\tau}$ specifies the τ th quantile of y_i and, as a consequence, the regression effects can be directly interpreted on the quantiles of the response distribution. Although we only consider here three specific quantiles of interest, estimation for a dense set of quantiles would allow us to characterise the complete distribution of the responses in terms of covariates (see, e.g. Bondell et al.; 2010; Schnabel and Eilers; 2013; Rodrigues et al.; 2019).

In the Bayesian framework, a specific distribution for the errors is required to facilitate full posterior inference. For this purpose, the asymmetric Laplace distribution (ALD) $y_i \sim \text{ALD}(\eta_{i,\tau}, \delta^2, \tau)$ with location predictor $\eta_{i,\tau}$, scale parameter δ^2 , asymmetry parameter τ and density

$$p(y_i | \eta_{i,\tau}, \delta^2, \tau) = \tau(1 - \tau)\delta^2 \exp(-\delta^2 \rho_\tau(y_i - \eta_{i,\tau}))$$

is particularly useful (Yu and Moyeed; 2001), since it can be shown to yield posterior mode estimates that are equivalent to the minimisers of (1). However, estimation with the ALD directly is not straightforward due to the non-differentiability of the check function $\rho_\tau(\cdot)$ at zero. Instead, to make Bayesian inference efficient, several authors considered re-writing the ALD as a scale mixture of two Gaussian distributions (Reed and Yu; 2009; Kozumi and Kobayashi; 2011; Yue and Rue; 2011; Lum and Gelfand; 2012; Waldmann et al.; 2013). Specifically, Tsionas (2003) show that

$$Y = \eta + \xi W + \sigma Z \sqrt{\delta^{-2} W}, \quad W \sim \mathbf{Exp}(\delta^2), \quad Z \sim \mathcal{N}(0, 1)$$

has an ALD distribution, where $\xi = \frac{1-2\tau}{\tau(1-\tau)}$, $\sigma = \frac{2}{\tau(1-\tau)}$ are two scalars depending on the quantile level τ ; and the random variables W , Z are independently distributed according to exponential ($\mathbf{Exp}(\delta^2)$ with rate δ^2) and standard Gaussian ($\mathcal{N}(0, 1)$) distributions, respectively. We assume a conjugate gamma prior distribution $\delta^2 \sim \mathcal{Ga}(a_\delta, b_\delta)$. This representation as a mixture facilitates an easy way to construct Gibbs sampling for MCMC inference, see Section 3.5 below.

We last note that other than the ALD are used in the literature to perform Bayesian quantile regression. For instance, Kottas and Krnjajić (2009) construct a generic class of semi-parametric and non-parametric distributions for the likelihood using Dirichlet process mixture models, while Reich et al. (2009) consider a flexible infinite mixture of Gaussian combined with a stick-breaking construction for the priors. However, we follow Yue and Rue (2011) along with the ALD since it facilitates Bayesian inference and computation in the additive models of this paper; and because Yue and Rue (2011) show empirically, that the ALD is flexible enough to capture various deviations from normality (such as skewness, heavy tails, etc.).

3.2 Semi-parametric predictors

In the following we present the formulation in the most general case to have a clear image of the generality of our proposal. Later, when we restrict to the application we will set a particular case, for example, all our covariates (except year-specific dummies) are subject to selection and there are no one free of selection. Also, we only consider splines for continuous covariates since we do not have random effects/spatial effects.

The predictors $\eta_{i,\tau}$ are decomposed into $\eta_{i,\tau} = \eta_{i,\tau}^{\text{in}} + \eta_{i,\tau}^{\text{sel}}$, i.e. a sub-predictor $\eta_{i,\tau}^{\text{sel}}$ being subject to explicit effect selection via spike and slab priors, and a second sub-predictor $\eta_{i,\tau}^{\text{in}}$ containing effects not subject to selection. We assume that $\eta_{i,\tau}^{\text{sel}}$ and $\eta_{i,\tau}^{\text{in}}$ are disjoint. The separation into two subsets of effects allows us to include specific covariate effects mandatory in the model (e.g. based on prior knowledge or since these represent confounding effects that have to be included in the model). We then model the predictors in a structured additive fashion along the lines of Fahrmeir et al. (2004)

$$\eta_{i,\tau} = \sum_{l=1}^{L_\tau} f_{l,\tau}^{\text{in}}(\boldsymbol{\nu}_i) + \sum_{j=1}^{J_\tau} f_{j,\tau}^{\text{sel}}(\boldsymbol{\nu}_i),$$

where the effects $f_{j,\tau}^{\text{sel}}(\boldsymbol{\nu}_i)$ and $f_{l,\tau}^{\text{in}}(\boldsymbol{\nu}_i)$ represent various types of flexible functions depending on (different subsets of) the covariate vector $\boldsymbol{\nu}_i$ that are to be selected via spike and slab priors and those not subject to selection, respectively. In the following, we focus on the specification of effect selection priors for $f_{j,\tau}^{\text{sel}}(\boldsymbol{\nu}_i)$ since in our application no specific functional forms of one of the nine covariates should a priori be excluded from selection. For a short period of time, it is assumed that there is no much uncertainty amongst the years, and we can safely consider the *year* as a fixed effect covariate. Estimation of the corresponding coefficients is handled as done in Waldmann et al. (2013).

In STAQ models it is assumed that each effect j in quantile τ , $f_{j,\tau}$, can be modelled as

$$f_{j,\tau}(\boldsymbol{\nu}_i) = \sum_{d=1}^D \beta_{j,k,d} B_{j,\tau,d}(\boldsymbol{\nu}_i),$$

where $B_{j,\tau,d}(\boldsymbol{\nu}_i)$, $d = 1, \dots, D$ are appropriate basis functions and $\boldsymbol{\beta}_{j,\tau} = (\beta_{j,\tau,1}, \dots, \beta_{j,\tau,D})'$ is the vector of unknown basis coefficients.

Scalar parameter expansion for effect selection To decide now for the overall relevance of $f_{j,\tau}$ in (3.1), we follow Klein et al. (2021) and others and reparameterise the equation above

to

$$f_{j,\tau}(\boldsymbol{\nu}_i) = \zeta_{j,\tau} \sum_{d=1}^D \tilde{\beta}_{j,\tau,d} B_{j,\tau,d}(\boldsymbol{\nu}_i),$$

where now $\tilde{\boldsymbol{\beta}}_{j,\tau} = (\tilde{\beta}_{j,\tau,1}, \dots, \tilde{\beta}_{j,\tau,D})'$ is the (standardised) vector of basis coefficients, and $\zeta_{j,\tau}$ is a scalar importance parameter. The latter is assigned a spike and slab prior in the next subsection (more precisely we place the prior on the squared importance parameter $\zeta_{j,\tau}^2$). This allows us to remove the effect from the predictor for $\zeta_{j,\tau}$ close to zero, while the effect is considered to be of high importance if $\zeta_{j,\tau}$ is large in absolute terms. Hence, instead of doing selection directly on the (possibly high-dimensional) vector $\boldsymbol{\beta}_{j,\tau}$ we can boil down the problem of selection on scalar parameters. This is reasonable due to the aim to select an effect with a corresponding vector $\boldsymbol{\beta}_{j,\tau}$ as a whole rather than single coefficients.

Relevant examples Due to the linear basis representation, the vector of function evaluations $\mathbf{f}_{j,\tau} = (f(\boldsymbol{\nu}_{j,\tau,1}), \dots, f(\boldsymbol{\nu}_{j,\tau,n}))'$ can now be written as $\mathbf{f}_{j,\tau} = \zeta_{j,\tau} \mathbf{B}_{j,\tau} \tilde{\boldsymbol{\beta}}_{j,\tau}$ where $\mathbf{B}_{j,\tau}$ is the $(n \times D)$ design matrix arising from the evaluation of the basis functions $B_{j,\tau,d}(\boldsymbol{\nu}_i)$, $d = 1, \dots, D$ at the observed $\boldsymbol{\nu}_1, \dots, \boldsymbol{\nu}_n$. While the STAR/STAQ framework enables a variety of different effect types, in the following we briefly discuss some details on linear and non-linear effects of univariate continuous covariates only (as these are the ones important in our application), while we refer the reader to Wood (2017) for more terms, such as spatial effects or random effects. The basis functions $\mathbf{B}_{j,\tau}$ depend very much on the type of effect (linear/non-linear) we are considering for the covariates.

For *linear effects* of continuous covariates, the columns of the design matrix $\mathbf{B}_{j,\tau}$ are equal to the different covariates. For binary/categorical covariates, the basis functions represent the chosen coding, e.g. dummy or effect coding and the design matrix then consists of the resulting dummy or effect coding columns.

For a *non-linear effect of a continuous covariate* we employ Bayesian P-splines (Lang and Brezger; 2004). The i th row of the design matrix $\mathbf{B}_{j,\tau}$ then contains the B-spline basis functions $B_{j,k,1}(x_i), \dots, B_{j,k,D}(x_i)$ evaluated at the observed covariate value x_i . If not stated otherwise, we will use cubic B-splines with seven inner knots (resulting in effects of dimension $D = 9$). This choice turns out to be sufficiently large in our case. We compared this to $D = 22$ (20 inner knots) and $D = 42$ (40 inner knots) following the default values considered in Lang and Brezger (2004) and Eilers and Marx (1996) but found the smaller number to still ensure enough flexibility.

3.3 Hierarchical spike and slab prior for effect selection

Constraint prior for regression coefficients To enforce specific properties such as smoothness or shrinkage, we assume multivariate Gaussian priors for the scaled basis coefficients. Thus we consider the following prior for the vector of standardised basis coefficients $\tilde{\boldsymbol{\beta}}_{j,\tau}$

$$p(\tilde{\boldsymbol{\beta}}_{j,\tau}) \propto \exp\left(-\frac{1}{2}\tilde{\boldsymbol{\beta}}_{j,\tau}'\mathbf{K}_{j,\tau}\tilde{\boldsymbol{\beta}}_{j,\tau}\right) \mathbb{1}\left[\mathbf{A}_{j,\tau}\tilde{\boldsymbol{\beta}}_{j,\tau} = \mathbf{0}\right],$$

where $\mathbf{K}_{j,\tau} \in \mathbb{R}^{D_{j,\tau} \times D_{j,\tau}}$ denotes the prior precision matrix implementing the desired smoothness properties, and the indicator function $\mathbb{1}[\mathbf{A}_{j,\tau}\boldsymbol{\beta}_{j,\tau} = \mathbf{0}]$ is included to enforce linear constraints on the regression coefficients via the constraint matrix $\mathbf{A}_{j,\tau}$. The latter is typically used to remove identifiability problems from the additive predictor (e.g. by centering the additive components of the predictor) but can also be used to remove the partial impropriety from the prior that comes from a potential rank deficiency of $\mathbf{K}_{j,\tau}$ with $\text{rk}(\mathbf{K}_{j,\tau}) = \kappa_{j,\tau} \leq D_{j,\tau}$. Here, we specifically assume that the constraint matrix $\mathbf{A}_{j,\tau}$ is chosen such that all rank deficiencies in $\mathbf{K}_{j,\tau}$ are effectively removed by setting $\mathbf{A}_{j,\tau} = \text{span}(\ker(\mathbf{K}_{j,\tau}))$, where $\ker(\mathbf{K}_{j,\tau})$ denotes the null space of $\mathbf{K}_{j,\tau}$ and $\text{span}(\ker(\mathbf{K}_{j,\tau}))$ is a representation of the corresponding basis.

To select the prior precisions $\mathbf{K}_{j,\tau}$, we again consider the type of effect for the covariates. For *linear effects*, we choose $\mathbf{K}_{j,\tau} = \mathbf{I}$, while for a *non-linear effect of a continuous covariate* we employ a second order random walk prior in all our empirical applications. Removing all rank deficiencies does not only remove the non-proprity from the prior, but also allows to make the relation between the original and the parameter expansion more explicit and to perform effect decomposition for the components of the additive predictor.

Effect decomposition With the above assumption, for Bayesian P-splines with a second order random walk prior, the rank of the prior precision matrix is $\kappa_{j,\tau} = D - 2$ and the null space corresponds to constant and linear effects. Applying the constrained prior allows to select linear effects and non-linear deviations separately. In general, an effect $f_{j,\tau}(\boldsymbol{\nu})$ can be decomposed into one unpenalised component $f_{j,k,\text{unpenalized}}(\boldsymbol{\nu})$ that corresponds to the null space of the prior precision matrix and the penalised complement $f_{j,k,\text{penalized}}(\boldsymbol{\nu})$

$$f_{j,\tau}(\boldsymbol{\nu}) = f_{j,k,\text{unpenalized}}(\boldsymbol{\nu}) + f_{j,k,\text{penalized}}(\boldsymbol{\nu}).$$

To achieve separate effect selection for the two components of f , we assign distinct spike and slab priors (Klein et al.; 2021; Rossell and Rubio; 2019).

Scaled beta prime spike and slab prior on squared importance parameter We follow Klein et al. (2021) and place the following hierarchical prior specification on the squared importance parameter $\zeta_{j,\tau}^2$:

$$\begin{aligned}
\zeta_{j,\tau}^2 | \gamma_{j,\tau}, \psi_{j,\tau}^2 &\sim \mathcal{Ga}\left(\frac{1}{2}, \frac{1}{2r_{j,\tau}(\gamma_{j,\tau})\psi_{j,\tau}^2}\right) \\
\gamma_{j,\tau} | \omega_{j,\tau} &\sim \mathcal{Be}(\omega_{j,\tau}) \\
\psi_{j,\tau}^2 &\sim \mathcal{IG}(a_{j,\tau}, b_{j,\tau}) \\
\omega_{j,\tau} &\sim \mathcal{Beta}(a_{0,j,\tau}, b_{0,j,\tau}) \\
r_{j,\tau} \equiv r(\gamma_{j,\tau}) &= \begin{cases} r_{j,\tau} > 0 \text{ small} & \gamma_{j,\tau} = 0 \\ 1 & \gamma_{j,\tau} = 1, \end{cases}
\end{aligned} \tag{2}$$

where $\mathcal{Ga}(a, b)$ denotes a gamma distribution with shape and scale parameters a, b , $\mathcal{Be}(p)$ is a Bernoulli distribution with success probability p , $\mathcal{IG}(a, b)$ is an inverse gamma distribution with parameters a, b and $\mathcal{Beta}(a, b)$ reads a beta distribution with shape parameters a, b .

The general idea of this prior hence relies on a mixture of one prior concentrated around zero such that it can effectively be thought of as representing zero (the spike component) and a more dispersed, mostly noninformative prior (the slab), and specified via the hierarchy. Specifically, the scale parameter $\psi_{j,\tau}^2$ determines the prior expectation of $\zeta_{j,\tau}^2$, which is $\psi_{j,\tau}^2$ for $\gamma_{j,\tau} = 1$ and $r_{j,\tau}\psi_{j,\tau}^2$ for $\gamma_{j,\tau} = 0$ with $r_{j,\tau} \ll 1$ being a fixed small value; hence the indicator $\gamma_{j,\tau}$ determines whether a specific effect $\beta_{j,\tau} = \tau_{j,\tau}\tilde{\beta}_{j,\tau}$ is included in the model ($\gamma_{j,\tau} = 1$) or excluded from the model ($\gamma_{j,\tau} = 0$). The parameter $\omega_{j,\tau}$ is the prior probability for an effect being included in the model and the remaining parameters $a_{j,\tau}$, $b_{j,\tau}$, $a_{0,j,\tau}$, $b_{0,j,\tau}$ and $r_{j,\tau}$ are hyperparameters of the spike and slab prior. Prior elicitation for these parameters comes in detail in Section 3.4, while the other choices follow those of Klein et al. (2021) and are derived from the theoretical results investigated in this paper and Pérez et al. (2017).

3.4 Prior elicitation

We now briefly outline prior elicitation for the hyperparameters $a_{j,\tau}$, $b_{j,\tau}$, $a_{0,j,\tau}$, $b_{0,j,\tau}$ and $r_{j,\tau}$. Pérez et al. (2017) show that the moments of order less than $a_{j,\tau}$ exist and the variance decreases with $a_{j,\tau}$. Furthermore, for small values of $a_{j,\tau}$, the spike and the slab component

will overlap such that moves from $\gamma_{j,\tau} = 0$ to $\gamma_{j,\tau} = 1$ are possible. We follow previous authors and set $a_{j,\tau} = 5$ as a default.

Since we do not have specific prior information about the prior inclusion probability of effects, we use $a_{j,0,\tau} = b_{0,j,\tau} = 1$, which corresponds to a flat prior on the unit interval. In general we note that prior assumptions can be implemented, since $\mathbb{P}(\gamma_{j,\tau} = 1 | a_{0,j,\tau}, b_{0,j,\tau}) = a_0 / (a_{0,j,\tau} + b_{0,j,\tau})$.

For the elicitation of $b_{j,\tau}$ and $r_{j,\tau}$, we use a more efficient procedure of what is done in Klein et al. (2021), an approach which itself is based on prior work of Simpson et al. (2017) and Klein and Kneib (2016). More precisely, we consider marginal probability statements on the supremum norm of $f_{j,\tau}$, $\|f_{j,\tau}\|_\infty$, and conditional on the status of the inclusion/exclusion parameter $\gamma_{j,\tau}$. Given $\gamma_{j,\tau} = 1$ (inclusion of the effect), the marginal distribution of $f_{j,\tau}(\boldsymbol{\nu})$ does no longer depend on $r_{j,\tau}$, such that the parameter $b_{j,\tau}$ can be determined from

$$\mathbb{P}(\|f_{j,\tau}\|_\infty \leq c_{j,\tau} \mid \gamma_{j,\tau} = 1) = \alpha_{j,\tau}. \quad (3)$$

This is the probability that the supremum norm of an effect is smaller than a pre-specified level $c_{j,\tau}$. Given $\gamma_{j,\tau} = 1$, $\alpha_{j,\tau}$ and $c_{j,\tau}$ should be small, reflecting the prior beliefs of the unlikely event that $\|f_{j,\tau}\|_\infty$ was smaller than $c_{j,\tau}$ if it was indeed an informative effect to be included into the predictor. Both the level $c_{j,\tau}$ and the prior probability $\alpha_{j,\tau}$ have to be specified by the analyst according to concrete prior beliefs. To derive $r_{j,\tau}$, we proceed similarly but considering the reverse scenario summarised via the probability

$$\mathbb{P}(\|f_{j,\tau}\|_\infty \leq c_{j,\tau} \mid \gamma_{j,\tau} = 0) = 1 - \alpha_{j,\tau} \quad (4)$$

now conditioning on non-inclusion. Since in this case the probability of not exceeding the threshold $c_{j,\tau}$ should be large, the probability is reversed to $1 - \alpha_{j,\tau}$ for $\alpha_{j,\tau}$ still small. Note that the absolute value of the effects can be taken without loss of generality due to the centring constraint of each function to ensure identifiability.

The basic idea of (3)–(4) is that such prior statements can be much more easily elicited in applications. To now access these probabilities, we generate a large sample from the marginal distribution of $\sup_{\boldsymbol{\nu} \in \mathcal{D}} |f_{j,\tau}(\boldsymbol{\nu})|$ (the latter can be approximated via simulation from the full hierarchical model). While Klein et al. (2021) suggest solving (3) and (4) with respect to $r_{j,\tau}$ and $b_{j,\tau}$ (which can be done independently) numerically via a time consuming optimization procedure, we note that this can be made much more efficient by making use of the scaling property of the scaled beta prime distribution: As shown in Pérez et al. (2017), the marginal

priors of spike and the slab components (i.e. with $\psi_{j,\tau}^2$ integrated out) $p(\zeta_{j,\tau}^2 | \gamma_{j,\tau})$ are scaled beta prime distributions with shape parameters $1/2$ and $a_{j,\tau}$ and scale parameter $2r_{j,\tau}b_{j,\tau}$. Hence, $2r_{j,\tau}b_{j,\tau}\zeta_{j,\tau}^2 | \gamma_{j,\tau}$ has a beta prime distribution with shape parameters $1/2$ and $a_{j,\tau}$ ($\mathcal{BP}(1/2, a_{j,\tau})$) and computing the probability in (3) is equivalent to computing

$$\mathbb{P}(\|f_{j,\tau}\|_\infty \leq c_{j,\tau} \mid \gamma_{j,\tau} = 1) = \mathbb{P}\left(\left\|\tilde{\zeta}_{j,\tau}\mathbf{b}'\tilde{\boldsymbol{\beta}}_{j,\tau}\right\|_\infty \leq \frac{c_{j,\tau}}{\sqrt{2r_{j,\tau}b_{j,\tau}}} \mid \gamma_{j,\tau} = 1\right),$$

where we have defined $f_{j,\tau} = \zeta_{j,\tau}\mathbf{b}'\tilde{\boldsymbol{\beta}}_{j,\tau} = \sqrt{2r_{j,\tau}b_{j,\tau}}\tilde{\zeta}_{j,\tau}\mathbf{b}'\tilde{\boldsymbol{\beta}}_{j,\tau}$, and $\tilde{\zeta}_{j,\tau}$ is the square root of a $\mathcal{BP}(1/2, a_{j,\tau})$ -distributed random variable. As a consequence, no numerical optimization is needed but it suffices to i) generate a large sample from $\left\|\tilde{\zeta}_{j,\tau}\mathbf{b}'\tilde{\boldsymbol{\beta}}_{j,\tau}\right\|_\infty$, ii) determine its $\alpha_{j,\tau}$ -quantile q^* , and iii) set $r_{j,\tau}^*$ such that $c_{j,\tau}/r_{j,\tau}^* = q^*$. The equivalent procedure applies to solving (4).

The parameters $\alpha_{j,\tau}$ and $c_{j,\tau}$ are easy to interpret and better accessible to the analyst as compared to all hyperparameters in (2). Their specific choice can help to balance between the true positive and false negative rates of effect selection. For instance, choosing $\alpha_{j,\tau}$ and $c_{j,\tau}$ smaller, will yield more conservative, i.e. sparser models. Based on the simulation results of Klein et al. (2021) the default value of $\alpha_{j,\tau} = c_{j,\tau} = 0.1$ is used in our empirical analysis. Finally, all covariates subject to selection are standardised to the interval $[0, 1]$ since this facilitates prior elicitation and comparability across the covariates.

3.5 Posterior inference

One appealing property in our effect selection STAQ model compared to Klein et al. (2021) is the more efficient MCMC sampling scheme that does not require any Metropolis-Hastings steps for the regression coefficients $\boldsymbol{\beta}_{j,\tau}$ but all steps can be realised in Gibbs updates as follows. Let

$$\boldsymbol{\theta} = \{\boldsymbol{\beta}_{1,\tau}, \dots, \boldsymbol{\beta}_{J,\tau}, \zeta_{1,\tau}^2, \dots, \zeta_{J,\tau}^2, \gamma_{1,\tau}, \dots, \gamma_{J,\tau}, \psi_{1,\tau}, \dots, \psi_{J,\tau}, \omega_{1,\tau}, \dots, \omega_{J,\tau}, w_1, \dots, w_n, \delta^2\}$$

be the set of all model parameters, then the MCMC sampler can be summarised as follows.

MCMC Sampler for effect selection in STAQ models

At each MCMC sweep:

Step 1. For $j = 1, \dots, J$ generate from $p(\boldsymbol{\beta}_{j,\tau} \mid \boldsymbol{\theta} \setminus \boldsymbol{\beta}_{j,\tau})$.

Step 2. For $j = 1, \dots, J$ generate from $p(\zeta_{j,\tau} \mid \boldsymbol{\theta} \setminus \zeta_{j,\tau})$.

Step 3. For $j = 1, \dots, J$ generate from $p(\gamma_{j,\tau} \mid \boldsymbol{\theta} \setminus \gamma_{j,\tau})$.

Step 4. For $j = 1, \dots, J$ generate from $p(\psi_{j,\tau} | \boldsymbol{\theta} \setminus \psi_{j,\tau})$.

Step 5. For $j = 1, \dots, J$ generate from $p(\omega_{j,\tau} | \boldsymbol{\theta} \setminus \omega_{j,\tau})$.

Step 6. For $i = 1, \dots, n$ generate from $p(w_i | \boldsymbol{\theta} \setminus w_i)$.

Step 7. Generate from $p(\delta^2 | \boldsymbol{\theta} \setminus \delta^2)$.

The full conditional distributions for $\boldsymbol{\beta}_{j,\tau}$ are Gaussian distributions $\mathcal{N}(\boldsymbol{\mu}_{j,\tau}, \boldsymbol{\Sigma}_{j,\tau})$ due to the conjugate model hierarchy implied by the location-scale mixture representation and the Gaussian priors for $\boldsymbol{\beta}_{j,\tau}$. The mean $\boldsymbol{\mu}_{j,\tau}$ and covariance $\boldsymbol{\Sigma}_{j,\tau}$ are:

$$\begin{aligned}\boldsymbol{\mu}_{j,\tau} &= \boldsymbol{\Sigma}_{j,\tau}^{-1} \left(\frac{\delta^2}{\sigma^2} \mathbf{B}'_{j,\tau} \mathbf{D}_w^{-1} (\mathbf{y} - \xi \mathbf{w} - (\boldsymbol{\eta} - \mathbf{B}_{j,\tau} \boldsymbol{\beta}_{j,\tau})) \right) \\ \boldsymbol{\Sigma}_{j,\tau} &= \left(\mathbf{K}_{j,\tau} + \frac{\delta^2}{\sigma^2} \mathbf{B}'_{j,\tau} \mathbf{D}_w^{-1} \mathbf{B}_{j,\tau} \right)^{-1},\end{aligned}$$

where $\mathbf{w} = (w_1, \dots, w_n)'$ and $\mathbf{D}_w = \text{diag}(w_1, \dots, w_n)$. At Step 2, we note that $p(\zeta_{j,\tau}^2 | \boldsymbol{\beta}_{j,k}, \gamma_{j,\tau}, \psi_{j,\tau}^2)$ is a generalised inverse Gaussian distribution $\mathcal{GIG}(p, q, c)$, with $p = -0.5 \text{rk}(\mathbf{K}_{j,\tau}) + 0.5$, $q = 1/(r(\gamma_{j,\tau})\psi_{j,k}^2)$, $c = \boldsymbol{\beta}'_{j,\tau} \mathbf{K}_{j,\tau} \boldsymbol{\beta}_{j,\tau}$. For Steps 3–5 it is easy to show that

$$p(\gamma_{j,\tau} = 1 | \boldsymbol{\theta} \setminus \gamma_{j,\tau}) = \left(1 + \frac{\varphi(\zeta_{j,\tau}; 0; r_{j,\tau} \psi_{j,\tau}^2) (1 - \omega_{j,\tau})}{\varphi(\tau_{j,\tau}; 0; \psi_{j,\tau}^2) \omega_{j,\tau}} \right)^{-1},$$

with $\varphi(\cdot; \mu, \sigma^2)$ the density of a normal distribution with mean μ and variance σ^2 ; and

$$\begin{aligned}\psi_{j,\tau}^2 | \boldsymbol{\theta} \setminus \psi_{j,\tau}^2 &\sim \mathcal{IG} \left(a_{j,\tau} + 0.5, b_{j,\tau} + \frac{\tau_{j,\tau}^2}{2r_{j,\tau}(\gamma_{j,\tau})} \right) \\ \omega_{j,\tau} | \boldsymbol{\theta} \setminus \omega_{j,\tau} &\sim \mathcal{Beta}(a_{0,j,\tau} + \gamma_{j,\tau}, b_{0,j,\tau} + 1 - \gamma_{j,\tau}),\end{aligned}$$

To generate w_i , $i = 1, \dots, n$ at Step 6, we recall the i.i.d. exponential priors with rate δ^2 which implies full conditional distributions for the reciprocal weights which are inverse Gaussian:

$$w_i^{-1} | \boldsymbol{\theta} \setminus w_i \sim \text{InvGauss} \left(\sqrt{\frac{\xi^2 + 2\sigma^2}{(y_i - \eta_i)^2}}, \frac{\delta^2(\xi^2 + 2\sigma^2)}{\sigma^2} \right).$$

Finally, the full conditional distributions for δ^2 at Step 7 are gamma, i.e.

$$\delta^2 | \boldsymbol{\theta} \setminus \delta^2 \sim \mathcal{Ga} \left(a_\delta + \frac{3n}{2}, b_\delta + \frac{1}{2\sigma^2} \sum_{i=1}^n \frac{(y_i - \eta_i - \xi w_i)^2}{w_i} + \sum_{i=1}^n w_i \right).$$

Implementation Our approach is implemented in a developer version of the free software BayesX Belitz et al. (2015), which can be downloaded and compiled at www.bayesx.org.

4 Analysis on Madrid’s air pollution

While Sections 2.1 and 2.2 provide a motivation for the problem underlying air pollution data and present the data and some initial exploratory analysis, respectively, this Section details our results. We recall Table 1 shows a description and summary statistics of the continuous covariates (before standardisation to $[0, 1]$) and from which we can extract the full predictor specification

$$\eta_\tau = \sum_{k=0}^4 \beta_k + f_1(co) + f_2(o3) + f_3(prec) + f_4(temp) + f_5(vel) + f_6(racha) + f_7(pres_max) + f_8(pres_min) + f_9(traffic)$$

Here, $f_j = f_{j,\text{penalized}} + f_{j,\text{unpenalized}}$ has been decomposed into respective linear and non-linear parts for each covariate (subject to selection) and β_k , $k = 0, \dots, 3$ are the overall intercept and year-specific coefficients (not subject to selection). After inspection of Figures 1 and 2, we noted that NO2 distributions differ depending on the predictor values, and also show a non-Gaussian behaviour. We also underlined that the variance of NO2 increases with increasing traffic, and that the predictor O3 has a clear non-linear effect on NO2, while the one for traffic is rather linear.

In this line, we now discuss results for the conditional thresholds $\tau \in \{0.6, 0.8, 0.9\}$. Table 2 shows posterior mean inclusion probabilities of $f_{\text{unpenalized}}$ (linear parts) and $f_{\text{penalized}}$ (non-linear parts) for $\tau \in \{0.6, 0.8, 0.9\}$ (across columns 2–4). We say that an effect part should be included in the model if the corresponding posterior mean inclusion probability $\mathbb{P}(\gamma_{j,\tau} | \boldsymbol{\theta} \setminus \gamma_{j,\tau}) \geq 0.5$ (in bold in Table 2). In addition, Figures 3 to 5 show estimated posterior effects for $f_{\text{unpenalized}}$ (linear parts), $f_{\text{penalized}}$ (non-linear parts) and $f = f_{\text{penalized}} + f_{\text{unpenalized}}$ (linear parts+non-linear parts) for $\tau \in \{0.6, 0.8, 0.9\}$ (across columns 1–3) and for all nine covariates (row-wise). Shown are the posterior mean (solid lines) and 95% pointwise credible intervals (dashed lines).

We highlight the following results. CO (co) has a strong positive linear effect for $\tau = 0.6$, but is negligible for $\tau = 0.8, 0.9$. This indicates that CO contributes to the NO2 distribution in a linear form but only for lower thresholds. In contract, O3 ($o3$) is a good predictor with a clear non-linear effect for all three quantiles with a notable decreasing effect. This inverse relationship between NO2 and O3 is expected as we discussed in Section 2.1. However, the non-linear structure was not so apparent, and we are able to underpin it.

Covariate	$f_{\text{unpenalized}}/f_{\text{penalized}}$	$\tau = 0.6$	$\tau = 0.8$	$\tau = 0.9$
<i>co</i>	$f_{\text{unpenalized}}$ (lin)	1	0	0
<i>co</i>	$f_{\text{penalized}}$ (non-lin)	0.422	0.232	0.18
<i>o3</i>	$f_{\text{unpenalized}}$ (lin)	0	0	0
<i>o3</i>	$f_{\text{penalized}}$ (non-lin)	1	0.997	1
<i>prec</i>	$f_{\text{unpenalized}}$ (lin)	0	0	0
<i>prec</i>	$f_{\text{penalized}}$ (non-lin)	0.764	0.973	1
<i>temp</i>	$f_{\text{unpenalized}}$ (lin)	1	1	0
<i>temp</i>	$f_{\text{penalized}}$ (non-lin)	0.958	0.992	1
<i>vel</i>	$f_{\text{unpenalized}}$ (lin)	1	0	0
<i>vel</i>	$f_{\text{penalized}}$ (non-lin)	0.15	0.886	0.998
<i>racha</i>	$f_{\text{unpenalized}}$ (lin)	0	1	0
<i>racha</i>	$f_{\text{penalized}}$ (non-lin)	0.725	0.749	0.836
<i>pres_max</i>	$f_{\text{unpenalized}}$ (lin)	0	0	0
<i>pres_max</i>	$f_{\text{penalized}}$ (non-lin)	0.36	0.111	0.353
<i>pres_min</i>	$f_{\text{unpenalized}}$ (lin)	0	1	0
<i>pres_min</i>	$f_{\text{penalized}}$ (non-lin)	0.424	0.3	0.376
<i>traffic</i>	$f_{\text{unpenalized}}$ (lin)	0	1	0
<i>traffic</i>	$f_{\text{penalized}}$ (non-lin)	0.945	0.813	0.865

Table 2: Posterior mean inclusion probabilities of $f_{\text{unpenalized}}$ (linear parts) and $f_{\text{penalized}}$ (non-linear parts) for $\tau \in \{0.6, 0.8, 0.9\}$ (across columns 2–4). We say an effect part should be included in the model if the corresponding posterior mean inclusion probability $\mathbb{P}(\gamma_{j,\tau} | \boldsymbol{\theta} \setminus \gamma_{j,\tau}) \geq 0.5$.

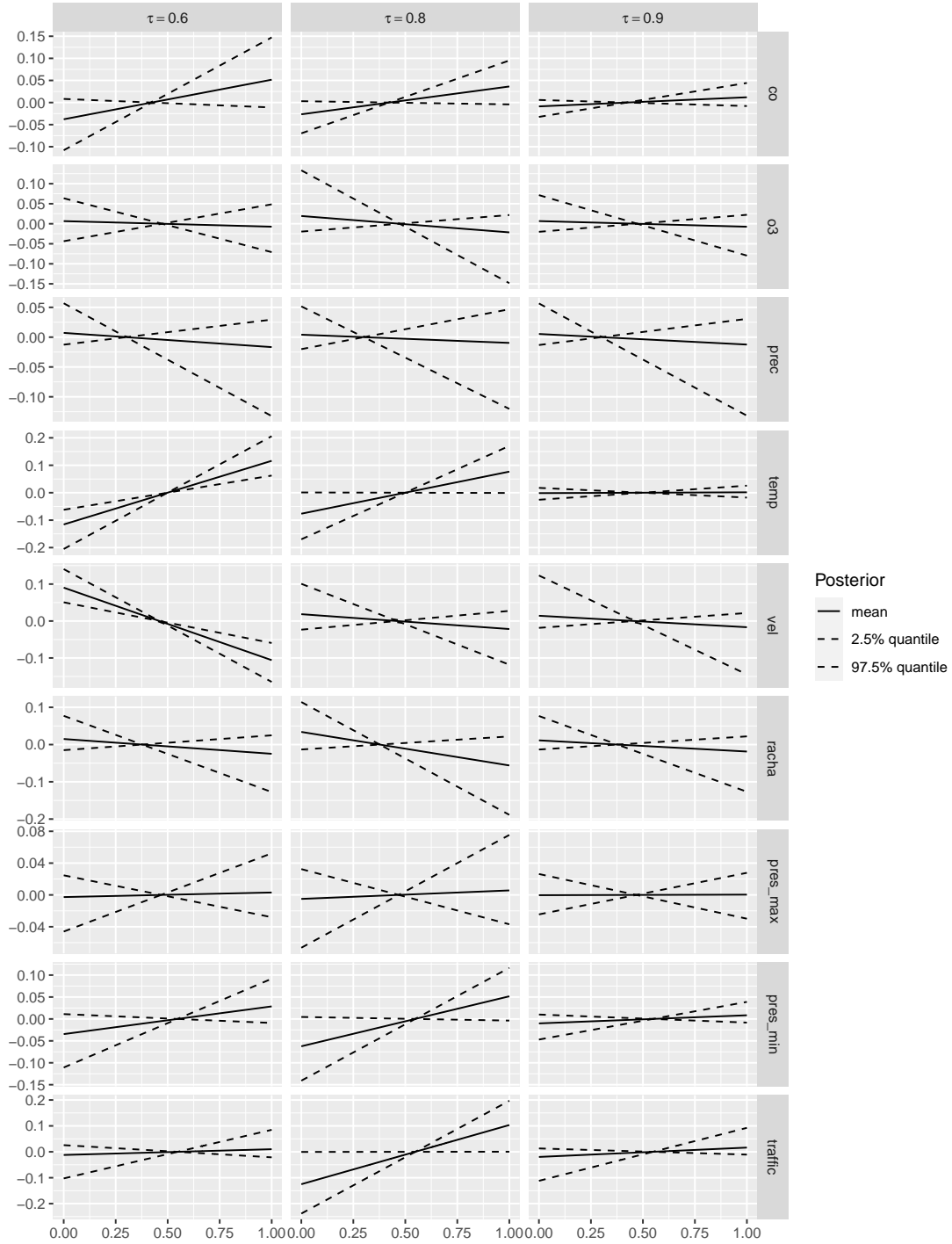


Figure 3: Estimated posterior effects for $f_{unpenalized}$ (linear parts) for $\tau \in \{0.6, 0.8, 0.9\}$ (across columns 1–3) and for all nine covariates (row-wise). Shown are the posterior mean (solid lines) and 95% pointwise credible intervals (dashed lines).

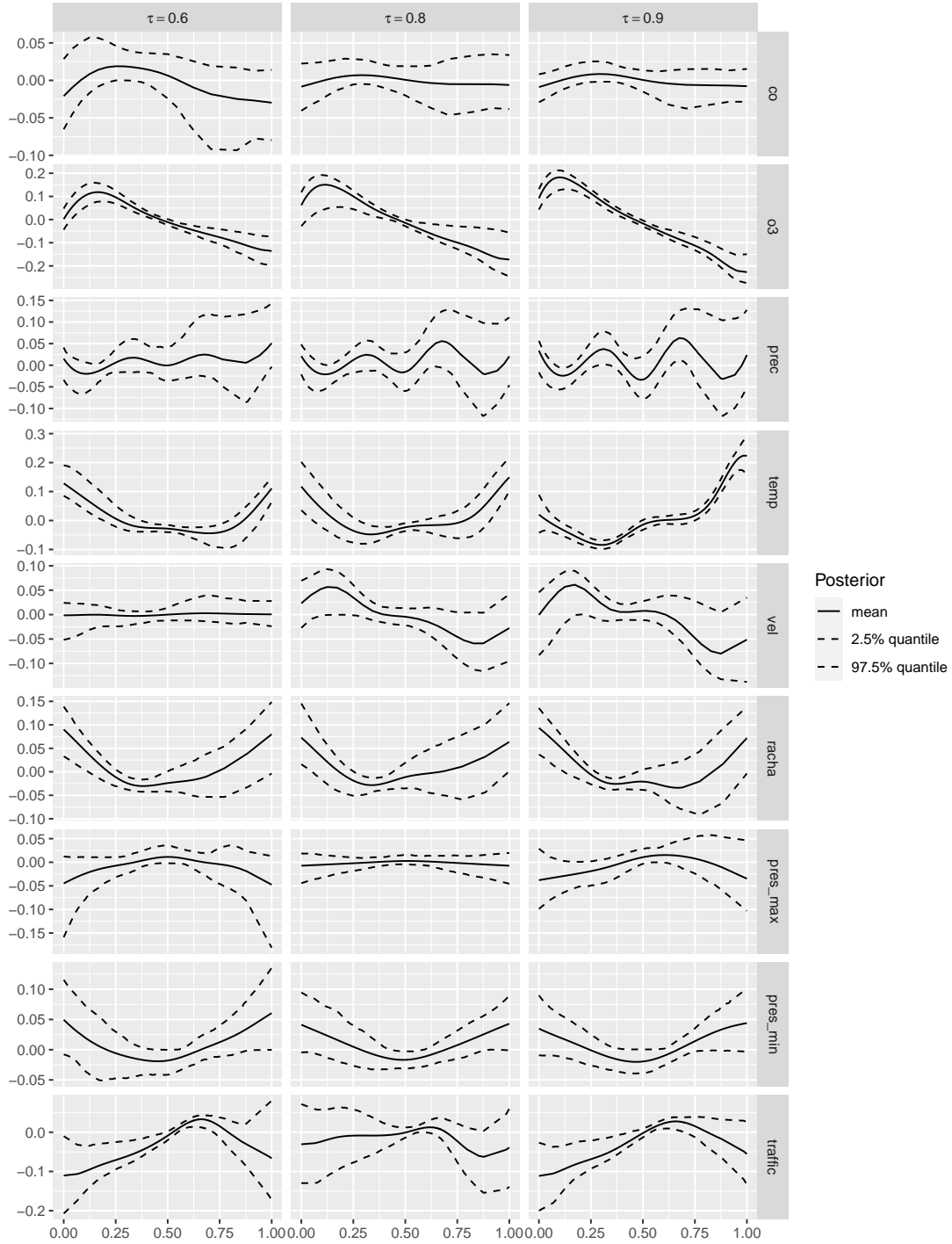


Figure 4: Estimated posterior effects for $f_{\text{penalized}}$ (non-linear parts) for $\tau \in \{0.6, 0.8, 0.9\}$ (across columns 1–3) and for all nine covariates (row-wise). Shown are the posterior mean (solid lines) and 95% pointwise credible intervals (dashed lines).

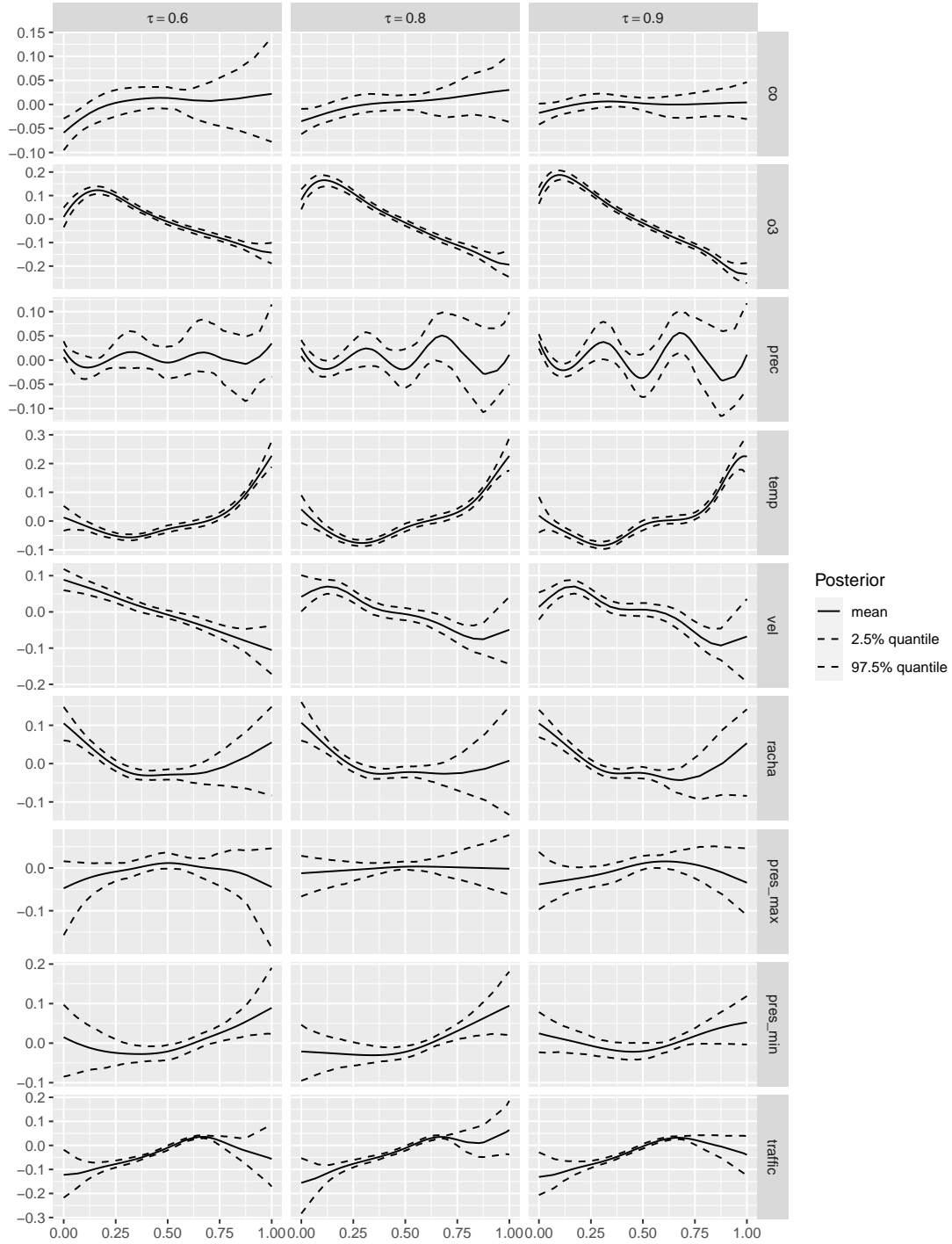


Figure 5: Estimated posterior effects for $f = f_{\text{penalized}} + f_{\text{unpenalized}}$ (linear parts+non-linear parts) for $\tau \in \{0.6, 0.8, 0.9\}$ (across columns 1-3) and for all nine covariates (row-wise). Shown are the posterior mean (solid lines) and 95% pointwise credible intervals (dashed lines).

Precipitation (*prec*) enters as a non-linear effect, and varies its strength depending on the quantile. In particular, the effect and its non-linearity is increasing with raising quantile τ . This combination of non-linear behaviour and increasing strength with raising quantiles brings a clear explanation of the effect of precipitation over NO2. Average temperature (*temp*) enters as both non-linear and linear effects for $\tau = 0.6, 0.9$ but only as a non-linear effect for $\tau = 0.8, 0.9$. Thus, the quantile has an effect on the dependence between NO2 and average temperature with the higher the temperature, the larger NO2.

Average wind speed (*vel*) enters as a non-linear effect for $\tau = 0.8, 0.9$ and linearly for $\tau = 0.6$. The linear effect for small thresholds is inverse indicating that with an increasing wind speed we get decreasing NO2 values. Importantly, for larger thresholds this linearity vanishes towards non-linear effects. When coming to maximum wind gusts (*racha*), the effects are basically non-linear for all quantiles. Air pressure (*pres_min*) is only relevant as a linear effect for $\tau = 0.8$ measured by minimum air pressure, but negligible for all other quantiles. Maximum pressure (*pres_max*) is however not selected.

Finally, average traffic flow (*traffic*) enters as a non-linear effect, with a stronger effect for $\tau = 0.6, 0.9$ and weaker effect for $\tau = 0.8$. This indicates that strong traffic congestions affect NO2 in a complicated non-linear fashion, but also this holds for lower thresholds, probably due to cross-relationships amongst some of the covariates. Latent (unobserved variables) also might place a hidden effect here, difficult to account for.

Noting that modelling reality of air pollution is certainly a critical, while complicated environmental problem, we have detected some functional forms, some of them highly non-linear, that underline the cross-relationships between a number of covariates and NO2. Chemical reactions are playing a role and make things even more complicated. Our statistical approach has been able to clarify some of these complicated relations.

5 Discussion and conclusions

This work fills the existing gap of methods for effect selection in semi-parametric quantile regression models. Inspired by the recent work of Klein et al. (2021) in the context of structured additive distributional regression (Klein et al.; 2015) our Bayesian effect selection approach for additive quantile regression employs a normal beta prime spike and slab prior on the scalar squared importance parameters associated with each effect part in the predictor. Compared to the distributional models of Klein et al. (2015) where predictors are placed on

the distributional parameters, our quantile regression is better interpretable as it allows to directly select certain effect types on conditional quantiles of a response and to decide whether relevant predictors affect the quantiles linearly or non-linearly. Other than in structured additive distributional regression, MCMC is extremely fast in our approach since all steps can be realised in Gibbs updates. Furthermore, we solve the large computational burden for eliciting the prior hyperparameters by making use of the scaling property of the (scaled) beta prime distribution.

While our method can be useful in a wide range of applications when interest is in understanding the impacts of influential covariates on the conditional distribution of a dependent variable beyond the mean, our methodological developments have specifically been stimulated the largest European environmental health risk, namely air pollution. Many European cities regularly exceed NO₂ limits and we consider one weather and pollution station in downtown of Madrid as a representative. We believe that we have better approximated the reality of air pollution detecting complicated linear and non-linear functional forms in combination with particular alarm thresholds. The results of this study are easily applicable to many other cities worldwide, perhaps with some adaptation and use of additional covariates. Indeed, our statistical approach enables to study quantile-specific covariate effects of any general functional form, and it helps deciding whether an effect should be included linearly, non-linearly or not at all in the relevant threshold quantiles.

We should note at this point that this paper only considers a representative station in a big city such as Madrid. The reason for this is that the focus of this paper is the analysis of the inherent relationships between a number of predictors and NO₂ to better understand the intrinsic mechanisms underlying air pollution, and the focus is not on prediction. These complicated mechanisms are missed out or simply not able to be understood by using other more widely encountered statistical approaches. We are also aware that there are more measuring stations spread through the city and the spatial structure could be relevant if the focus would be more on prediction of missing data, or prediction onto the future. We leave this important point for future extensions of our approach.

References

- Achakulwisut, P., Brauer, M., Hystad, P. and Anenberg, S. (2019). Global, national, and urban burdens of paediatric asthma incidence attributable to ambient NO₂ pollution: estimates from global datasets, *Lancet Planet Health* **3**(4): e166–e178.
- Airquality-News (2018). airqualitynews.com and <https://airqualitynews.com/2018/08/22/comeap-updates-estimates-on-uk-air-pollution-deaths/>, Accessed: 2021-05-20.
- Alhamzawi, R. (2015). Model selection in quantile regression models, *Journal of Applied Statistics* **42**(2): 445–458.
- Alhamzawi, R. and Yu, K. (2012). Variable selection in quantile regression via gibbs sampling, *Journal of Applied Statistics* **39**(4): 799–813.
- Alhamzawi, R. and Yu, K. (2013). Conjugate priors and variable selection for bayesian quantile regression, *Computational Statistics & Data Analysis* **64**: 209–219.
- Antanasijevic, D., Pocajt, V., Peric-Grujic, A. and Ristic, M. (2018). Multiple-input-multiple-output general regression neural networks model for the simultaneous estimation of traffic-related air pollutant emissions, *Atmospheric Pollution Research* **9**(2): 388–397.
- Belitz, C., Brezger, A., Klein, N., Kneib, T., Lang, S. and Umlauf, N. (2015). BayesX – Software for Bayesian inference in structured additive regression models, <http://www.bayesx.org>. *Version 3.0.2*.
- Bergantino, A., Bierlaire, M., Catalano, M., Migliore, M. and Amoroso, S. (2013). Taste heterogeneity and latent preferences in the choice behaviour of freight transport operators, *Transport Policy* **30**: 77–91.
- Bondell, H. D., Reich, B. J. and Wang, H. (2010). Noncrossing quantile regression curve estimation, *Biometrika* **97**(4): 825–838.
- Borge, R., Santiago, J., Paz, D., de la Martin, F., Domingo, J., Valdes, C., Sanchez, B., Rivas, E., Rozas, M. and Lazaro, S. (2018). Application of a short term air quality action plan in Madrid (Spain) under a high-pollution episode-part ii: Assessment from multi-scale modelling, *Science of Total Environment* **635**: 1574–1584.
- Catalano, M., Galatioto, F., Bell, M., Namdeo, A. and Bergantino, A. (2016). Improving the prediction of air pollution peak episodes generated by urban transport networks, *Environmental Science and Policy* **60**: 69–83.
- Clyde, M. and George, E. I. (2004). Model uncertainty, *Statistical Science* **19**(1): 81–94.
- EEA (2018). Air quality in Europe-2018 report, *European Environment Agency Technical report no 12/2018*.
- EEA (2020). Air pollution is the biggest environmental health risk in europe, <https://www.eea.europa.eu/themes/air/air-pollution-is-the-single>, Accessed: 2021-05-20.
- Eilers, P. H. C. and Marx, B. D. (1996). Flexible smoothing with B-splines and penalties, *Statistical Science* **11**(2): 89–121.
- Fahrmeir, L., Kneib, T. and Lang, S. (2004). Penalized structured additive regression for space-time data: A Bayesian perspective, *Statistica Sinica* **14**: 731–761.
- Fasiolo, M., Wood, S. N., Zaffran, M., Nedellec, R. and Goude, Y. (2020). Fast calibrated additive quantile regression, *Journal of the American Statistical Association* pp. 1–11.

- Fenske, N., Kneib, T. and Hothorn, T. (2011). Identifying risk factors for severe childhood malnutrition by boosting additive quantile regression, *Journal of the American Statistical Association* **106**: 494–510.
- George, E. and McCulloch, R. (1997). Approaches for Bayesian variable selection, *Statistica Sinica* **7**: 339–373.
- Hastie, T. J. and Tibshirani, R. J. (1990). *Generalized Additive Models*, Chapman & Hall/CRC, New York/Boca Raton.
- Hatzopoulou, M., Valois, M., Mihele, C., Lu, G., Bagg, S., Minet, L. and Brook, J. (2017). Robustness of land-use regression models developed from mobile air pollutant measurements, *Environmental Science Technology* **51**(7): 3938–3947.
- Klein, N., Carlan, M., Kneib, T., Lang, S. and Wagner, H. (2021). Bayesian effect selection in structured additive distributional regression models, *To appear in Bayesian Analysis*. doi:10.1214/20-BA1214, early view at <https://projecteuclid.org/euclid.ba/1592272906>.
- Klein, N. and Kneib, T. (2016). Scale-dependent priors for variance parameters in structured additive distributional regression, *Bayesian Analysis* **11**: 1107–1106.
- Klein, N., Kneib, T., Klasen, S. and Lang, S. (2015). Bayesian structured additive distributional regression for multivariate responses, *Journal of the Royal Statistical Society. Series C (Applied Statistics)* **64**: 569–591.
- Kneib, T. (2013). Beyond mean regression, *Statistical Modelling* **13**: 275–303.
- Koenker, R. (2005). *Quantile Regression*, Cambridge University Press, New York. Economic Society Monographs.
- Koenker, R. (2010). Additive models for quantile regression: An analysis of risk factors for malnutrition in india, in H. D. Vinod (ed.), *Advances in Social Science Research Using R*, Springer Verlag, pp. 23–33.
- Koenker, R. (2011). Additive models for quantile regression, *Brazilian Journal of Probability and Statistics* **25**: 239–262.
- Koenker, R. and Bassett, G. (1978). Regression quantiles, *Econometrica* **46**(1): 33–50.
- Kottas, A. and Krnjajić, M. (2009). Bayesian semiparametric modelling in quantile regression, *Scandinavian Journal of Statistics* **36**(2): 297–319.
- Kozumi, H. and Kobayashi, G. (2011). Gibbs sampling methods for Bayesian quantile regression, *Journal of Statistical Computation and Simulation* **81**(11): 1565–1578.
- Lang, S. and Brezger, A. (2004). Bayesian P-splines, *Journal of Computational and Graphical Statistics* **13**: 183–212.
- Lee, D., An, S., Song, H., Park, O., Park, K., Seo, G., Cho, Y. and Kim, E. (2014). The effect of traffic volume on the air quality at monitoring sites in Gwangju, *Korean Society of Environmental Health* **40**(3): 204–214.
- Lua, M., Schmitza, O., de Hoogh, K., Kaid, Q. and Karssen, D. (2020). Evaluation of different methods and data sources to optimise modelling of NO₂ at a global scale, *Environment International* **142**: 105856.
- Lum, K. and Gelfand, A. E. (2012). Spatial quantile multiple regression using the asymmetric Laplace process, *Bayesian Analysis* **7**(2): 235–258.
- McCullagh, P. and Nelder, J. A. (1989). *Generalized Linear Models*, 2nd edn, Chapman &

- Hall/CRC, New York/Boca Raton.
- Meinshausen, N. (2006). Quantile regression forests, *Journal of Machine Learning Research* **7**: 983–999.
- Meng, X., Chen, L., Cai, J., Zou, B., Wu, C.-F., Fu, Q., Zhang, Y., Liu, Y. and Kan, H. (2015). A land use regression model for estimating the NO₂ concentration in Shanghai, China, *Environmental Research* **137**: 308–315.
- Mitchell, T. and Beauchamp, J. J. (1988). Bayesian variable selection in linear regression, *Journal of the American Statistical Association* **83**: 1023 – 1032.
- O’Hara, R. and Sillanpää, M. (2009). A review of Bayesian variable selection methods: What, How, and Which, *Bayesian Analysis* **4**: 85–118.
- Pérez, M.-E., Pericchi, L. R. and Raméz, I. C. (2017). The scaled beta₂ distribution as a robust prior for scales, *Bayesian Analysis* **12**(3): 615–637.
- Perez, P. and Trier, A. (2001). Prediction of NO and NO₂ concentrations near a street with heavy traffic in Santiago, Chile, *Atmospheric Environment* **35**(10): 1783—1789.
- Prybutok, V., Yi, J. and Mitchell, D. (2000). Comparison of neural network models with arima and regression models for prediction of Houston’s daily maximum ozone concentrations, *European Journal of Operations Research* **122**: 31–40.
- Reed, C. and Yu, K. (2009). A partially collapsed Gibbs sampler for Bayesian quantile regression, *Technical Report available at <http://bura.brunel.ac.uk/handle/2438/3593>* .
- Reich, B. J., Bondell, H. D. and Wang, H. J. (2009). Flexible Bayesian quantile regression for independent and clustered data, *Biostatistics* **11**(2): 337–352.
- Rodrigues, T., Dortet-Bernadet, J.-L. and Fan, Y. (2019). Simultaneous fitting of Bayesian penalised quantile splines, *Computational Statistics & Data Analysis* **134**: 93–109.
- Rossell, D. and Rubio, F. J. (2019). Additive Bayesian variable selection under censoring and misspecification. arXiv:1907.13563.
- Ryu, J., Park, C. and Jeon, S. (2019). Mapping and statistical analysis of NO₂ concentration for local government air quality regulation, *Sustainability* **11**(14): 3809.
- Schnabel, S. K. and Eilers, P. H. C. (2013). Simultaneous estimation of quantile curves using quantile sheets, *ASTA Advances in Statistical Analysis* **97**(1): 77–87.
- Simpson, D., Rue, H. Martins, T. G., Riebler, A. and Sørbye, S. H. (2017). Penalising model component complexity: A principled, practical approach to constructing priors, *Statistical Science* **32**(1): 1–28.
- Tsionas, E. (2003). Bayesian quantile inference, *Journal of Statistical Computation and Simulation* **73**(9): 659–674.
- Urban-NO₂-Atlas (2019). <https://publications.jrc.ec.europa.eu/repository/handle/JRC118193>, Accessed: 2021-05-20.
- Valks, P., Pinardi, A., Richter, A., Lambert, J.-C., Hao, N., Loyola, D., van Roozendaal, M. and Emmadi, S. (2011). Operational total and tropospheric NO₂ column retrieval for GOME-2, *Atmospheric Measurement Technology* **4**(7): 1491–1514.
- Waldmann, E., Kneib, T., Yue, Y. R., Lang, S. and Flexeder, C. (2013). Bayesian semiparametric additive quantile regression, *Statistical Modelling* **13**(3): 223–252.
- WHO (2014). World Health Organization: Ambient (outdoor) air pollution in cities. <https://>

- [//www.who.int/airpollution/data/cities-2014/en/](http://www.who.int/airpollution/data/cities-2014/en/), Accessed: 2021-05-20.
- Wood, S. N. (2017). *Generalized Additive Models : An Introduction with R*, 2nd edn, Chapman & Hall/CRC.
- Wu, Y. and Liu, Y. (2009). Variable selection in quantile regression, *Statistica Sinica* **19**(2): 801–817.
- Yu, K., Chen, C., Reed, C. and Dunson, D. (2013). Bayesian variable selection in quantile regression, *Statistics and its Interface* **6**(2): 261–274.
- Yu, K. and Moyeed, R. A. (2001). Bayesian quantile regression, *Statistics & Probability Letters* **54**(4): 437–447.
- Yue, Y. R. and Rue, H. (2011). Bayesian inference for additive mixed quantile regression models, *Computational Statistics & Data Analysis* **55**(1): 84–96.